Rheologica Acta (2019) 58:699–707
https://doi.org/10.1007/s00397-019-01168-6

RAPID COMMUNICATION

Annular pressure-driven flow of a Bingham plastic with pressure-dependent rheological parameters

Iasonas Ioannou[1] · Georgios C. Georgiou[2]

Received: 27 March 2019 / Revised: 10 July 2019 / Accepted: 5 August 2019 / Published online: 24 August 2019

Abstract

The pressure and temperature dependence of the yield stress is well established in oil drilling. In the present work, the steady, annular pressure-driven flow of a Bingham plastic is considered under the assumption that both the plastic viscosity and the yield stress vary linearly with pressure. A semi-analytical solution is derived for the case where the growth coefficients of both rheological parameters are equal, which, for certain oil drilling fluids, is indeed a reasonable assumption allowing the existence of a separable solution with an annular unyielded core. The inner and outer radii of the unyielded core are determined by solving numerically an algebraic system of equations. The pressure, which is two-dimensional in the yielded parts of the domain, and the velocity, which varies only with the radius, are calculated by means of explicit analytical expressions. The conditions for the occurrence of flow and the effects of the growth coefficient and the radii ratio on the width of the unyielded annular plug, the velocity profiles, and the pressure distributions are discussed.

Keywords Bingham plastic · Annular Poiseuille flow · Pressure-dependent viscosity · Pressure-dependent yield stress

Introduction

Viscoplastic or yield stress materials, such as colloidal gels, emulsions, soft glassy materials, and jammed colloidal suspensions, behave as solids below a critical applied stress, i.e., the yield stress τ_y^*, and as fluids otherwise (Frigaard 2019). As a result, the flow domain consists of the so-called unyielded $\left(\tau^* \le \tau_y^*\right)$ and yielded $\left(\tau^* > \tau_y^*\right)$ zones. It should be noted that throughout the paper starred symbols denote dimensional quantities. Determining the interfaces between yielded and unyielded regions is not a trivial task, especially in two- and three-dimensional flows and/or in time-dependent flows (Saramito and Wachs 2017; Damianou et al. 2016; Huilgol et al. 2019). Different methods have been proposed in order to tackle this problem, the two most popular being the regularization and the augmented Lagrangian methods (Saramito and Wachs 2017). A nice article about simple (i.e., non-thixotropic and inelastic) yield stress fluids and their usefulness has been recently published by Frigaard (2019).

In most studies of isothermal flows of yield stress materials, the rheological parameters are commonly assumed to be constant. Such an assumption, however, is not valid in many important applications involving high pressure differences, e.g., in polymer processing, in tribology, in microfluidics, in oil drilling and transport, and in lava and pyroclastic flows (Málek et al. 2007; Panaseti et al. 2018; Frigaard 2019). In the literature of the mechanics of solid and granular materials (Ionescu et al. 2015) and in oil drilling (Coussot 2014; Hermoso et al. 2014), it is well established that the yield stress depends not only on the temperature but also on the pressure. The dependence on the latter becomes more important in processes involving big pressure differences. In order to describe the isothermal yield stress behavior of two drilling fluids, Hermoso et al. (2014) employed the following linear equation

$$\tau_y^*\left(p^*\right) = \tau_0^*\left[1 + \beta^*\left(p^* - p_0^*\right)\right] \tag{1}$$

where τ_0^* denotes the yield stress at a reference pressure p_0^* and β^* is the yield stress growth coefficient. As for

✉ Georgios C. Georgiou
georgios@ucy.ac.cy

Iasonas Ioannou
iasonasce@gmail.com

[1] Department of Mechanical and Process Engineering, ETH Zurich, Sonneggstrasse 3, 8092 Zurich, Switzerland

[2] Department of Mathematics and Statistics, University of Cyprus, P.O. Box 20537, 1678 Nicosia, Cyprus

the plastic viscosity, Hermoso and co-workers used the Barus equation

$$\mu^*(p^*) = \mu_0^* e^{\alpha^*(p^*-p_0^*)} \tag{2}$$

where μ_0^* is the plastic viscosity at the reference pressure and $\alpha^* \geq 0$ is the plastic viscosity growth coefficient (Barus 1893). The linearized version of Eq. (2)

$$\mu^*(p^*) = \mu_0^*\left[1+\alpha^*(p^*-p_0^*)\right] \tag{3}$$

may also be used if the pressure-dependence of μ^* is weak ($\alpha^* \ll 1$); the encountered pressures are not extremely high and remain always above the reference pressure. It is clear that the latter limitation also holds for the linear expression for the yield stress. As pointed out by Fusi and Rosso (2018), when referring to "pressure," we actually mean the "mean normal stress" of the fluid, which should not be confused with the Lagrange multiplier due to the compressibility constraint.

Damianou and Georgiou (2017) analyzed the plane Poiseuille flow of a Bingham plastic with pressure-dependent material parameters assuming that the yield stress and the plastic viscosity obey respectively Eqs. (1) and (3). In this case, the tensorial form of the Bingham plastic constitutive equation reads

$$\begin{cases} \mathbf{D}^* = \mathbf{0}, & \tau^* \leq \tau_y^*(p^*) \\ \boldsymbol{\tau}^* = 2\left[\dfrac{\tau_0^*\left[1+\beta^*(p^*-p_0^*)\right]}{\dot{\gamma}^*} + \mu_0^*\left[1+\alpha^*(p^*-p_0^*)\right]\right]\mathbf{D}^*, & \tau^* > \tau_y^*(p^*) \end{cases} \tag{4}$$

where $\boldsymbol{\tau}^*$ is the viscous stress tensor,

$$\mathbf{D}^* \equiv \frac{1}{2}\left[\nabla^*\mathbf{v}^* + (\nabla^*\mathbf{v}^*)^T\right] \tag{5}$$

is the rate of deformation tensor, $\mathbf{v}^*$ is the velocity vector, $\dot{\gamma}^* \equiv \sqrt{\mathrm{tr}\mathbf{D}^{*2}/2}$ and $\tau^* \equiv \sqrt{\mathrm{tr}\boldsymbol{\tau}^{*2}/2}$. It is readily seen that when $\alpha^* = \beta^* = 0$, Eq. (5) is reduced to the classic Bingham plastic constitutive equation with constant material parameters. In their analysis, Damianou and Georgiou (2017) made use of the integral formulation for the momentum equation in the unyielded core, as proposed by Fusi et al. (2015). They reported explicit solutions for the velocity, the pressure, and the width of the central unyielded region, which is constant despite the pressure-dependence of the material parameters. This is not the case in the axisymmetric Poiseuille flow where an analytical solution can be derived only when the growth coefficients a^* and β^* are equal, as pointed out in our recent work (Ioannou and Georgiou 2018), where it has been shown that the radius of the unyielded core is constant. In a subsequent work, Housiadas et al. (2018) modeled the lubrication of a Bingham plastic in long tubes using the approach proposed by Fusi and Farina (2018) in order to investigate the general case of the axisymmetric viscoplastic flow with pressure-dependent rheological parameters. It was demonstrated that the shape of the central unyielded core depends on the relative values of α^* and β^*. More specifically, the unyielded core is conical, contracting when $\beta^* < a^*$ and expanding when $\beta^* > a^*$, while it remains cylindrical when $\beta^* = a^*$. Fusi and Rosso (2018) have also considered the axisymmetric Poiseuille flow of a Herschel-Bulkley fluid the material constants of which, however, are zero at the reference pressure and then increase linearly with pressure; as a result, the derived solutions cannot be reduced to the classical viscoplastic flow with constant rheological parameters.

The objective of the present work is to investigate the annular, pressure-driven flow of a Bingham plastic with material parameters varying linearly with pressure following Eq. (4), as a natural extension of the above-mentioned studies. The aforementioned flow is encountered in the petroleum industry, e.g., drilling muds, which exhibit yield stress, are used in long annular tubes where high pressures are necessary in maintaining the flow [7]. The plastic viscosity and yield stress growth parameters are assumed to be equal, which is indeed a reasonable assumption for certain oil drilling fluids (Hermoso et al. 2014; Ioannou and Georgiou 2018). Ioannou and Georgiou (2018) calculated the values of α^* and β^* corresponding to the data of Hermoso et al. (2014) for the B34-based drilling fluid at different temperatures demonstrating that these are of the same order, with values in the range of 10^{-8}–10^{-7} Pa^{-1}.

In the following sections, the governing equations for the annular flow of a Bingham plastic with pressure-dependent material parameters are presented. It is demonstrated in particular that a separable solution exists only in the special case where $\alpha^* = \beta^*$. This analytical solution is derived next, extending thus the analytical solution for the classical Bingham plastic model (Bird et al. 1982; Chatzimina et al. 2007).

Governing equations

We consider the Poiseuille flow, of a material obeying Eq. (4), in a horizontal annulus of length L^* and radii κR^* and R^*, where $0 < \kappa < 1$. We work in cylindrical coordinates, as illustrated in Fig. 1. Under the assumption that the flow is unidirectional with $v_z^* = v_z^*(r^*)$ and $v_r^* = 0$, the continuity equation is automatically satisfied and the unyielded core is an annulus. Hence, the flow field consists of three annular regions, i.e., two yielded regions, denoted by I and II, and the intermediate unyielded region III, the radii of which are denoted by σ_i^* and σ_o^*, where $\kappa R^* < \sigma_i^* < \sigma_o^* < R^*$ (see Fig. 1).

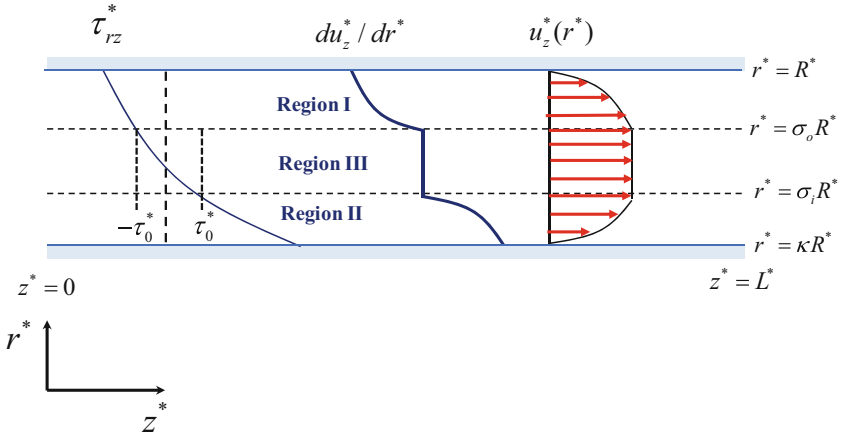

Fig. 1 Geometry of the flow with some symbol definitions and a sketch of the velocity profile

The problem is dedimensionalised by scaling z^* by L^*, r^*, σ_i^*, and σ_o^* by R^*, v_z^* by $\tau_0^* R^*/\mu_0^*$, τ_{rz}^* by τ_o^*, and $(p^*-p_o^*)$ by τ_0^*/ε, where

$$\varepsilon \equiv \frac{R^*}{L^*} \tag{6}$$

is the aspect ratio. Hereafter, the dimensionless equations are dropping the stars. In both yielded regions, i.e., for $(z, r) \in [0, 1] \times [\sigma_o, 1] \cup [0, 1] \times [\kappa, \sigma_i]$, the pressure is two-dimensional, i.e., $p = p(z, r)$ and τ_{rz} is the only non-zero component of the stress tensor:

$$\tau_{rz} = \operatorname{sgn}\left(\frac{dv_z}{dr}\right)(1+\beta p) + (1+\alpha p)\frac{dv_z}{dr} \tag{7}$$

where

$$\alpha \equiv \frac{\alpha^* \tau_0^*}{\varepsilon}, \quad \beta \equiv \frac{\beta^* \tau_0^*}{\varepsilon} \tag{8}$$

are the dimensionless plastic viscosity and yield stress growth numbers and $\operatorname{sgn}(dv_z^*/dr^*)$ is -1 and 1 in regions I and II, respectively. The dimensionless z- and r-components of the momentum equation read

$$-\frac{\partial p}{\partial z} + \frac{1}{r}\frac{\partial (r\tau_{rz})}{\partial r} = 0 \tag{9}$$

and

$$-\frac{\partial p}{\partial r} + \varepsilon^2 \frac{\partial \tau_{rz}}{\partial z} = 0 \tag{10}$$

respectively. On the annular walls, the usual no-slip conditions are assumed, i.e., $v_z(1) = v_z(\kappa) = 0$. On the yield surfaces, the velocity is constant given by $v_z(\sigma_o) = v_z(\sigma_i) = v_c$, where v_c is the constant velocity of the plug core, $\Omega = \{(z, r) : \ z \in [0, 1], r \in [\sigma_i, \sigma_o], \theta \in [0, 2\pi]\}$, which moves as a solid body.

Moreover, in the rigid core, the pressure is one-dimensional, $p_c = p_c(z)$ satisfying $p_c(0) = \Delta p$ $p_c(1) = 0$, where Δp is the imposed dimensionless pressure at the inlet. For steady-state flow in the absence of body forces, the integral balance of linear momentum of the whole plug core yields (Fusi et al., 2015; Fusi and Rosso 2018):

$$\int_{\partial\Omega} (-p\mathbf{I} + \boldsymbol{\tau})\cdot\mathbf{n} dS = 0 \tag{11}$$

where $\mathbf{n}$ is the outward unit normal to the boundary $\partial\Omega$ and $\mathbf{I}$ is the unit tensor. The radial component of Eq. (11) is automatically satisfied due to symmetry, while the longitudinal component becomes:

$$2\int_0^1 \left(\sigma_o \tau_{rz}|_{r=\sigma_o} - \sigma_i \tau_{rz}|_{r=\sigma_i}\right) dz + \left(\sigma_o^2 - \sigma_i^2\right)\Delta p = 0 \tag{12}$$

Since the rate of strain (velocity gradient) vanishes at the two yield surfaces, Eq. (7) yields

$$\tau_{rz}|_{r=\sigma_o} = -\tau_{rz}|_{r=\sigma_i} = 1 + \beta p_c \tag{13}$$

Substituting Eq. (13) into Eq. (12) and simplifying, we get

$$\sigma_o - \sigma_i = \frac{2}{\Delta p}\left(1 + \beta \int_0^1 p_c dz\right) \tag{14}$$

In yielded region I, i.e., for $(z, r) \in [0, 1] \times [\sigma_o, 1]$, the dimensionless shear stress is given by

$$\tau_{rz} = -(1+\beta p) + (1+\alpha p)\frac{dv_z}{dr} \tag{15}$$

Substituting Eq. (15) into Eqs. (9) and (10), we get

$$\frac{\partial p}{\partial z} = \left(\alpha \frac{dv_z}{dr} - \beta\right)\frac{\partial p}{\partial r} + (1+\alpha p)\frac{d^2 v_z}{dr^2} + \frac{-(1+\beta p) + (1+ap)\dfrac{dv_z}{dr}}{r} \tag{16}$$

and

$$\frac{\partial p}{\partial r} = \varepsilon^2 \left(\alpha \frac{dv_z}{dr} - \beta\right)\frac{\partial p}{\partial z} \tag{17}$$

Substituting Eq. (17) into Eq. (16) and moving terms involving the velocity to the RHS, one gets:

$$\frac{\partial p/\partial z}{1+\alpha p} = \frac{d^2v_z/dr^2 + (1/r)dv_z/dr}{1-\varepsilon^2(\alpha dv_z/dr-\beta)^2} - \frac{1/r}{1-\varepsilon^2(\alpha dv_z/dr-\beta)^2}\frac{1+\beta p}{1+\alpha p} \tag{18}$$

Similarly, in yielded region II, i.e., for $(z, r) \in [0, 1] \times [\kappa, \sigma_i]$, where

$$\tau_{rz} = (1+\beta p) + (1+\alpha p)\frac{dv_z}{dr} \tag{19}$$

we get

$$\frac{\partial p/\partial z}{1+\alpha p} = \frac{d^2v_z/dr^2 + (1/r)v_z/dr}{1-\varepsilon^2(\alpha dv_z/dr+\beta)^2} + \frac{1/r}{1-\varepsilon^2(\alpha dv_z/dr+\beta)^2}\frac{1+\beta p}{1+\alpha p} \tag{20}$$

It is readily observed that in both yielded regions, variables can be separated, and an analytical solution can be obtained only in the special case where $a = \beta$. This solution is derived below.

In the unyielded region III, i.e., for $(z, r) \in [0, 1] \times [\sigma_i, \sigma_o]$, the rate-of-strain is zero. Therefore, the unyielded core moves as a solid at constant velocity and thus

$$v_z(r = \sigma_o) = v_z(r = \sigma_i) = v_c \tag{21}$$

Analytical solution for $\alpha = \beta$

Region I

When $a = \beta$, Eq. (18) is simplified as follows:

$$\frac{\partial p/\partial z}{1+\alpha p} = \frac{d^2v_z/dr^2 + (1/r)dv_z/dr - 1/r}{1-\varepsilon^2\alpha^2(dv_z/dr-1)^2} = -\Lambda_1 \tag{22}$$

where Λ_1 is a positive constant to be determined. Given that the pressure is strictly decreasing function of the axial distance, the RHS of Eq. (22) has been chosen to have a minus sign. Solving for v_z and applying the boundary conditions $dv_z/dr(r = \sigma_o) = v_z(r = 1) = 0$, we get:

$$v_z(r) = -\frac{1}{\varepsilon^2\alpha^2\Lambda_1}\ln\left[\frac{I_o(\varepsilon a\Lambda_1 r) + c_1K_o(\varepsilon a\Lambda_1 r)}{I_o(\varepsilon a\Lambda_1) + c_1K_o(\varepsilon a\Lambda_1)}\right] - (1-r), \quad \sigma_o \le r \le 1 \tag{23}$$

where I_o and K_o are the modified Bessel functions of first and second kind, respectively, and

$$c_1 = \frac{I_1(\varepsilon a\Lambda_1\sigma_o) - \varepsilon a I_o(\varepsilon a\Lambda_1\sigma_o)}{K_1(\varepsilon a\Lambda_1\sigma_o) + \varepsilon a K_o(\varepsilon a\Lambda_1\sigma_o)} \tag{24}$$

Integrating now the differential equation for the pressure in Eq. (22) yields

$$p(r, z) = \frac{1}{\alpha}\left[w_1(r)e^{-\alpha\Lambda_1 z} - 1\right], \quad \sigma_o \le r \le 1 \tag{25}$$

where $w_1(r)$ is an unknown function. Substituting p and v_z into Eq. (18), we get a first-order differential equation for w_1,

$$w_1'(r) - \varepsilon\alpha\Lambda_1\frac{[I_1(\varepsilon a\Lambda_1 r) - c_1K_1(\varepsilon a\Lambda_1 r)]}{[I_o(\varepsilon a\Lambda_1 r) + c_1K_o(\varepsilon a\Lambda_1 r)]}w_1(r) = 0 \ , \tag{26}$$

the general solution of which is

$$w_1(r) = C_1[I_o(\varepsilon a\Lambda_1 r) + c_1K_o(\varepsilon a\Lambda_1 r)] \tag{27}$$

where C is an integration constant. Applying the conditions $p(0, \sigma_o) = \Delta p$ and $p(1, \sigma_o) = 0$ gives

$$C_1 = \frac{1+\alpha\Delta p}{I_o(\varepsilon a\Lambda_1\sigma_o) + cK_o(\varepsilon a\Lambda_1\sigma_o)} \quad \text{and} \quad \Lambda_1 = \frac{\ln(1+\alpha\Delta p)}{\alpha} \tag{28}$$

Therefore, we have:

$$p(z, r) = \frac{1}{\alpha}\left[(1+\alpha\Delta p)^{1-z}\frac{I_o(\varepsilon a\Lambda_1 r) + c_1K_o(\varepsilon a\Lambda_1 r)}{I_o(\varepsilon a\Lambda_1\sigma_o) + c_1K_o(\varepsilon a\Lambda_1\sigma_o)} - 1\right], \quad \sigma_o \le r \le 1 \tag{29}$$

Region II

Working as in region I, solving again for v_z and applying the boundary conditions $dv_z/dr(r = \sigma_i) = v_z(r = \kappa) = 0$, we get

$$v_z(r) = -\frac{1}{\varepsilon^2\alpha^2\Lambda_2}\ln\left[\frac{I_o(\varepsilon a\Lambda_2 r) + c_2K_o(\varepsilon a\Lambda_2 r)}{I_o(\varepsilon a\Lambda_2\kappa) + c_2K_o(\varepsilon a\Lambda_2\kappa)}\right] + (\kappa - r), \quad \kappa \le r \le \sigma_i \tag{30}$$

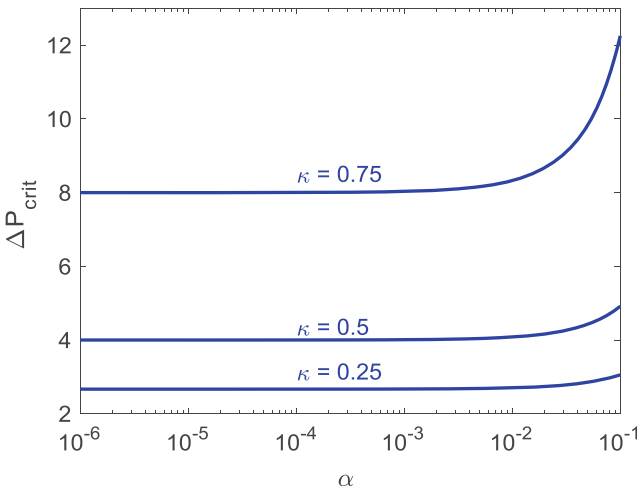

Fig. 2 Variation of the critical pressure difference $\Delta p_{crit} \equiv \Delta p^*_{crit}/(\tau_0^* L^*/R^*)$ required for the initiation of the annular Bingham plastic flow with the growth parameter α for different values of κ

where

$$c_2 = \frac{I_1(\varepsilon a\Lambda_2\sigma_i) + \varepsilon a I_o(\varepsilon a\Lambda_2\sigma_i)}{K_1(\varepsilon a\Lambda_2\sigma_i) - \varepsilon a K_o(\varepsilon a\Lambda_2\sigma_i)} \tag{31}$$

Integrating for pressure and applying the conditions $p(0,\sigma_i)=\Delta p$ and $p(1,\sigma_i)=0$ gives

$$p(z,r) = \frac{1}{\alpha}\left[(1+\alpha\Delta p)^{1-z}\frac{I_o(\varepsilon a\Lambda_2 r) + c_2 K_o(\varepsilon a\Lambda_2 r)}{I_o(\varepsilon a\Lambda_2\sigma_i) + c_2 K_o(\varepsilon a\Lambda_2\sigma_i)} - 1\right], \quad \kappa \le r \le \sigma_i \tag{32}$$

It turns out that the constant Λ_2 is equal to Λ_1; hence, the symbol Λ will be used hereafter for both constants:

$$\Lambda = \Lambda_1 = \Lambda_2 = \frac{\ln(1+\alpha\Delta p)}{\alpha} \tag{33}$$

Region III

It can be deduced from either Eq. (29) or Eq. (32) that the pressure in the unyielded core is

$$p_c(z) = \frac{1}{\alpha}\left[(1+\alpha\Delta p)^{1-z} - 1\right], \quad \sigma_i \le r \le \sigma_o \tag{34}$$

Substituting into Eq. (14), we get

$$\sigma_o - \sigma_i = \frac{2\alpha}{\ln(1+\alpha\Delta p)} = \frac{2}{\Lambda} \tag{35}$$

The second equation needed for the calculation of the radii σ_i and σ_o of the unyielded annular core is obtained by

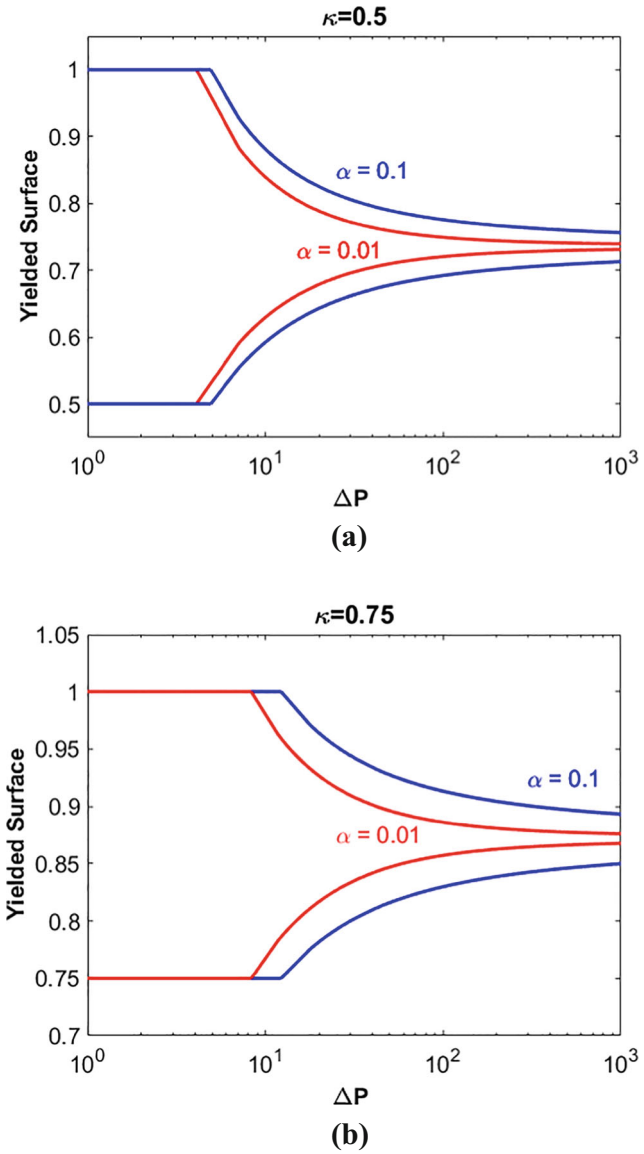

Fig. 3 Radii of the unyielded annular core versus $\Delta p \equiv \Delta p^* / \left(\tau_0^*/\varepsilon\right)$ for $\varepsilon = 0.01$ and $\alpha = 0.01$ and 0.1: **a** $\kappa = 0.5$; **b** $\kappa = 0.75$

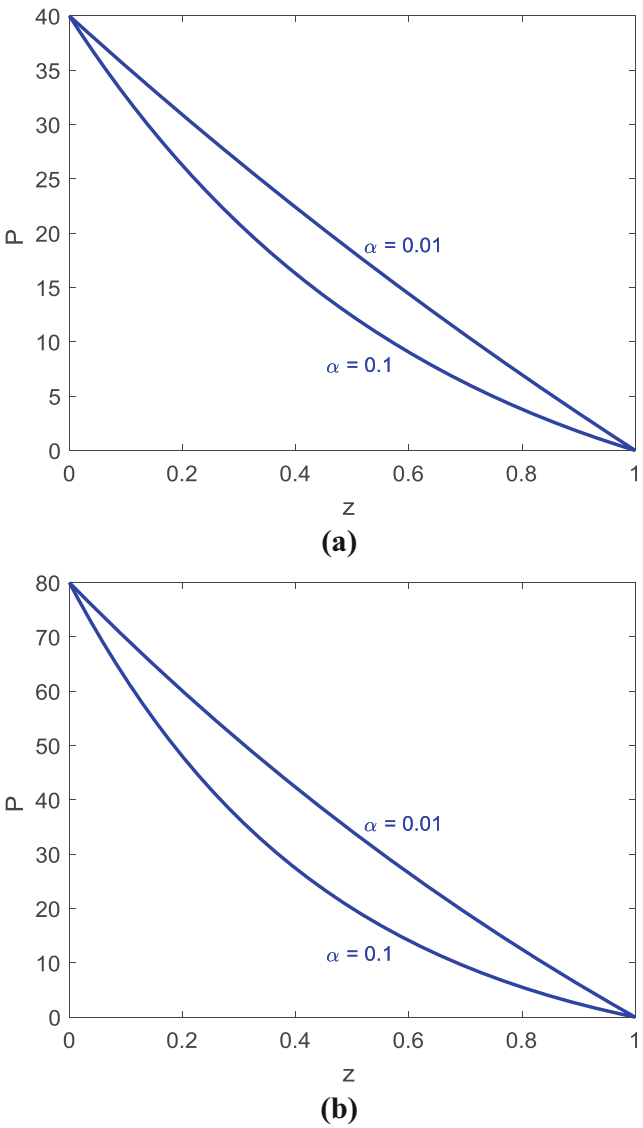

Fig. 4 Dimensionless pressure in the unyielded core (where the pressure is one-dimensional depending only on the axial distance z) for $\alpha = 0.01$ and 0.1: **a** $\Delta p = 40$; **b** $\Delta p = 60$

demanding that Eq. (21) be satisfied. Substituting Eqs. (32) and (33) into Eq. (21) yields:

$$\frac{(\sigma_o-\sigma_i)}{2\varepsilon^2\alpha^2}\left[\ln\left(\frac{I_o(\varepsilon a\Lambda\sigma_o)+c_1K_o(\varepsilon a\Lambda\sigma_o)}{I_o(\varepsilon a\Lambda)+c_1K_o(\varepsilon a\Lambda)}\right)-\ln\left(\frac{I_o(\varepsilon a\Lambda\sigma_i)+c_2K_o(\varepsilon a\Lambda\sigma_i)}{I_o(\varepsilon a\Lambda\kappa)+c_2K_o(\varepsilon a\Lambda\kappa)}\right)\right]-(1+\kappa-\sigma_o-\sigma_i)=0 \tag{36}$$

In summary, when $a=\beta>0$ the velocity profile and the pressure are given by:

$$v_z(r)=\begin{cases}-\frac{(\sigma_o-\sigma_i)}{2\varepsilon^2\alpha^2}\ln\left(\frac{I_o(\varepsilon a\Lambda r)+c_1K_o(\varepsilon a\Lambda r)}{I_o(\varepsilon a\Lambda)+c_1K_o(\varepsilon a\Lambda)}\right)-(1-r), & \sigma_o\le r\le 1\\ -\frac{(\sigma_o-\sigma_i)}{2\varepsilon^2\alpha^2}\ln\left(\frac{I_o(\varepsilon a\Lambda\sigma_o)+c_1K_o(\varepsilon a\Lambda\sigma_o)}{I_o(\varepsilon a\Lambda)+c_1K_o(\varepsilon a\Lambda)}\right)-(1-\sigma_o), & \sigma_i\le r\le\sigma_o\\ -\frac{(\sigma_o-\sigma_i)}{2\varepsilon^2\alpha^2}\ln\left(\frac{I_o(\varepsilon a\Lambda r)+c_2K_o(\varepsilon a\Lambda r)}{I_o(\varepsilon a\Lambda\kappa)+c_2K_o(\varepsilon a\Lambda\kappa)}\right)+\kappa-r, & \kappa\le r\le\sigma_i\end{cases} \tag{37}$$

and

$$p(z,r)=\frac{1}{\alpha}\begin{cases}\left[(1+\alpha\Delta p)^{1-z}\frac{I_o(\varepsilon a\Lambda r)+c_1K_o(\varepsilon a\Lambda r)}{I_o(\varepsilon a\Lambda\sigma_o)+c_1K_o(\varepsilon a\Lambda\sigma_o)}-1\right], & \sigma_o\le r\le 1\\ \left[(1+\alpha\Delta p)^{1-z}-1\right], & \sigma_i\le r\le\sigma_o\\ \left[(1+\alpha\Delta p)^{1-z}\frac{I_o(\varepsilon a\Lambda r)+c_2K_o(\varepsilon a\Lambda r)}{I_o(\varepsilon a\Lambda\sigma_i)+c_2K_o(\varepsilon a\Lambda\sigma_i)}-1\right], & \kappa\le r\le\sigma_i\end{cases} \tag{38}$$

The oilfield industry used to rely on simplified two-dimensional plane flow slot models to represent flow in an annulus, at least when the radii ratio κ is not too far from unity. It is straightforward to demonstrate that when the annular gap is small compared with the outer radius, the above solution reduces to the two-dimensional solution reported by Damianou and Georgiou (2017).

When $a=\beta=0$, the solution derived by Bird et al. (1982) for the special case where the rheological parameters are pressure independent is recovered. The velocity and the pressure are respectively given by

$$v_z(r)=\begin{cases}-\sigma_o\ln r+\frac{\Delta p}{4}\left(1-r^2+2\sigma_o{}^2\ln r\right)-(1-r), & \sigma_o\le r\le 1\\ -\sigma_o\ln\sigma_o+\frac{\Delta p}{4}\left(1-\sigma_o{}^2+2\sigma_o{}^2\ln\sigma_o\right)-(1-\sigma_o), & \sigma_i\le r\le\sigma_o\\ \sigma_i\ln\left(\frac{r}{\kappa}\right)+\frac{\Delta p}{4}\left(\kappa^2-r^2+2\sigma_i{}^2\ln\left(\frac{r}{\kappa}\right)\right)+\kappa-r, & \kappa\le r\le\sigma_i\end{cases} \tag{39}$$

and

$$p(z)=\Delta p\,(1-z),\quad \kappa\le r\le 1 \tag{40}$$

while σ_i and σ_o are calculated by solving the system of

$$\sigma_o-\sigma_i=\frac{2}{\Delta p} \tag{41}$$

and

$$-\left(\sigma_o\ln\sigma_o+\sigma_i\ln\left(\frac{\sigma_i}{\kappa}\right)\right)+\frac{\Delta p}{4}\left(1-\sigma_o{}^2(1-2\ln\sigma_o)-\kappa^2+\sigma_i{}^2\left(1-2\ln\left(\frac{\sigma_i}{\kappa}\right)\right)\right)-(1+\kappa-\sigma_o-\sigma_i)=0 \tag{42}$$

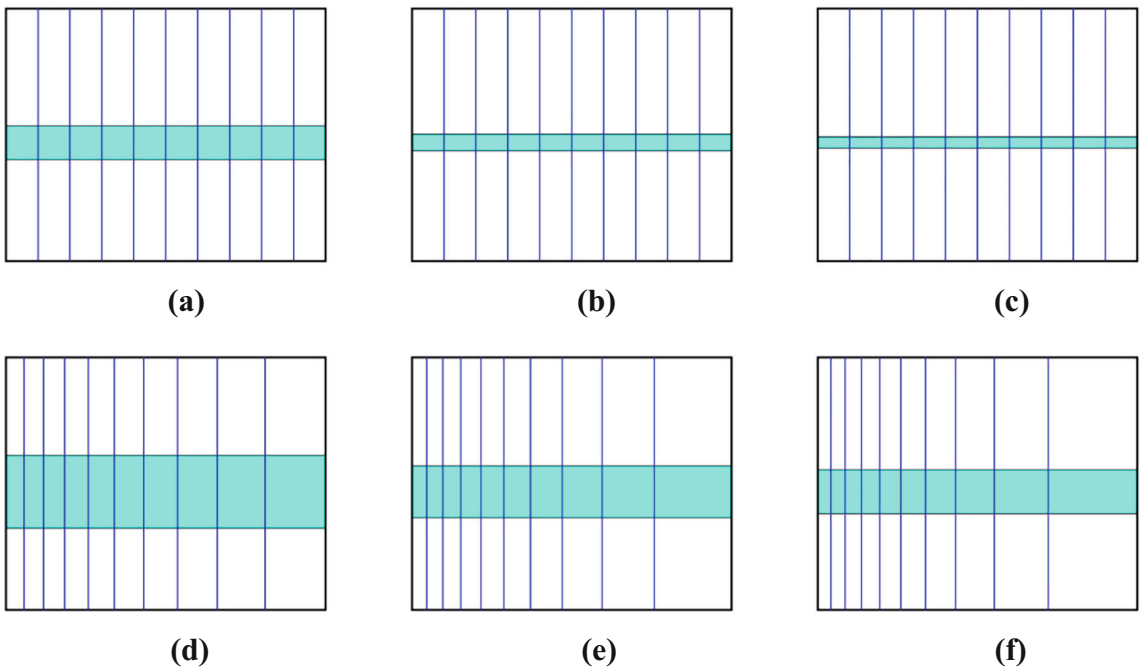

Fig. 5 Effect of the growth parameter α on the pressure contours for $\kappa=0.5$ and $\varepsilon=0.01$: **a** $\alpha=0$, $\Delta p=30$; **b** $\alpha=0$, $\Delta p=60$; **c** $\alpha=0$, $\Delta p=90$; **d** $\alpha=0.1$, $\Delta p=30$; **e** $\alpha=0.1$, $\Delta p=60$; **f** $\alpha=0.1$, $\Delta p=90$; the flow is from left to right with $z\in[0,1]$ and $r\in[\kappa,1]$

Substituting Eq. (41) into Eqs. (39) and (42) yields the expressions reported by Chatzimina et al. (2007).

Results and discussion

The critical pressure difference required to start the flow can be found from Eqs. (35) or (41) as the pressure difference at which $\sigma_o = 1$ and $\sigma_i = \kappa$:

$$\Delta p_{\text{crit}} = \begin{cases} \frac{1}{\alpha}\left(e^{2\alpha/(1-\kappa)}-1\right), & \alpha > 0 \\ \frac{2}{1-\kappa}, & \alpha = 0 \end{cases} \tag{43}$$

The effects of the growth number α and the aspect ratio κ on Δp_{crit} are illustrated in Fig. 2. As expected, Δp_{crit} increases with α when κ is fixed. At higher values of κ, the variation of Δp_{crit} with α becomes more significant and the critical pressure difference is shifted to higher values rapidly. The variation of the radii of the unyielded annular core, σ_o and σ_i, with the pressure difference Δp is illustrated in Fig. 3 for $\alpha =$ 0.01, 0.1 and $\kappa =$ 0.5 and 0.75. Below the critical pressure difference Δp_{crit}, there is no flow and thus $\sigma_o = 1$ and $\sigma_i = \kappa$. Once the critical value is exceeded, σ_o decreases and σ_i increases with Δp. The rates of these changes are reduced with α. As the imposed pressure difference Δp is increased, the two radii converge to the radius at which the Newtonian velocity profile in the same geometry attains its maximum.

It should be noted that the values of α and ε are much smaller than unity. Using the values calculated by Ioannou and Georgiou (2018) for the B34-based drilling fluid studied by Hermoso et al. (2014) and taking $\varepsilon = 0.0001$ as a representative aspect ratio (Azar and Roberto Samuel 2007), one finds that the value of α is in the range $3\ 10^{-6}$–$3\ 10^{-5}$. In what

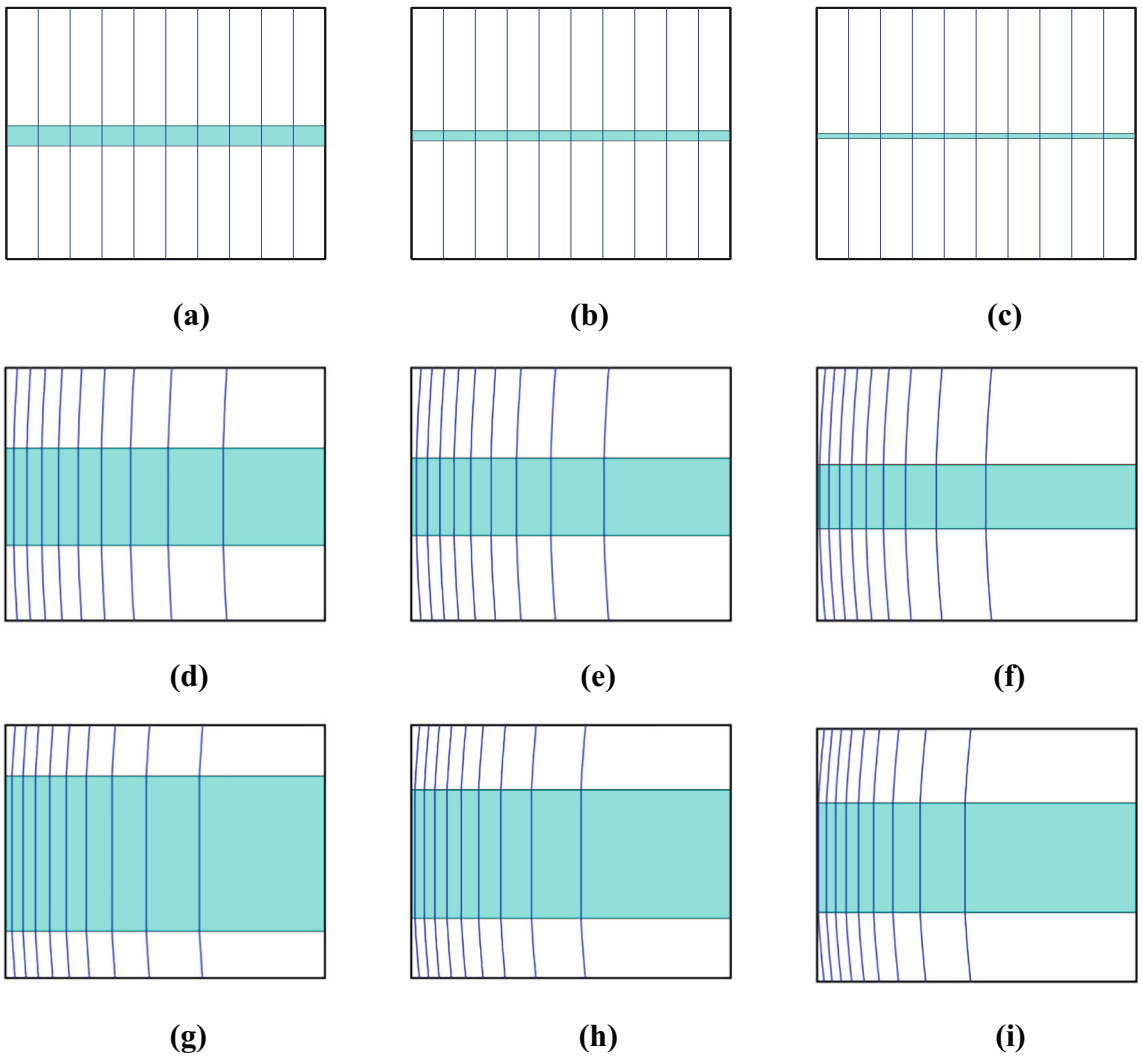

Fig. 6 Effect of the growth parameter α on the pressure contours for $\kappa =$ 0.8 and $\varepsilon = 1$: **a** $\alpha = 0$, $\Delta p = 125$; **b** $\alpha = 0.1$, $\Delta p = 250$; **c** $\alpha = 0.1$, $\Delta p =$ 500; **d** $\alpha = 0.1$, $\Delta p = 125$; **e** $\alpha = 0.1$, $\Delta p = 250$; **f** $\alpha = 0.1$, $\Delta p = 500$; **g** $\alpha = 0.2$, $\Delta p = 125$; **h** $\alpha = 0.2$, $\Delta p = 250$; **i** $\alpha = 0.2$, $\Delta p = 500$; high values of ε and α were chosen in order to exaggerate the differences. The flow is from left to right with $z \in [0, 1]$ and $r \in [\kappa, 1]$

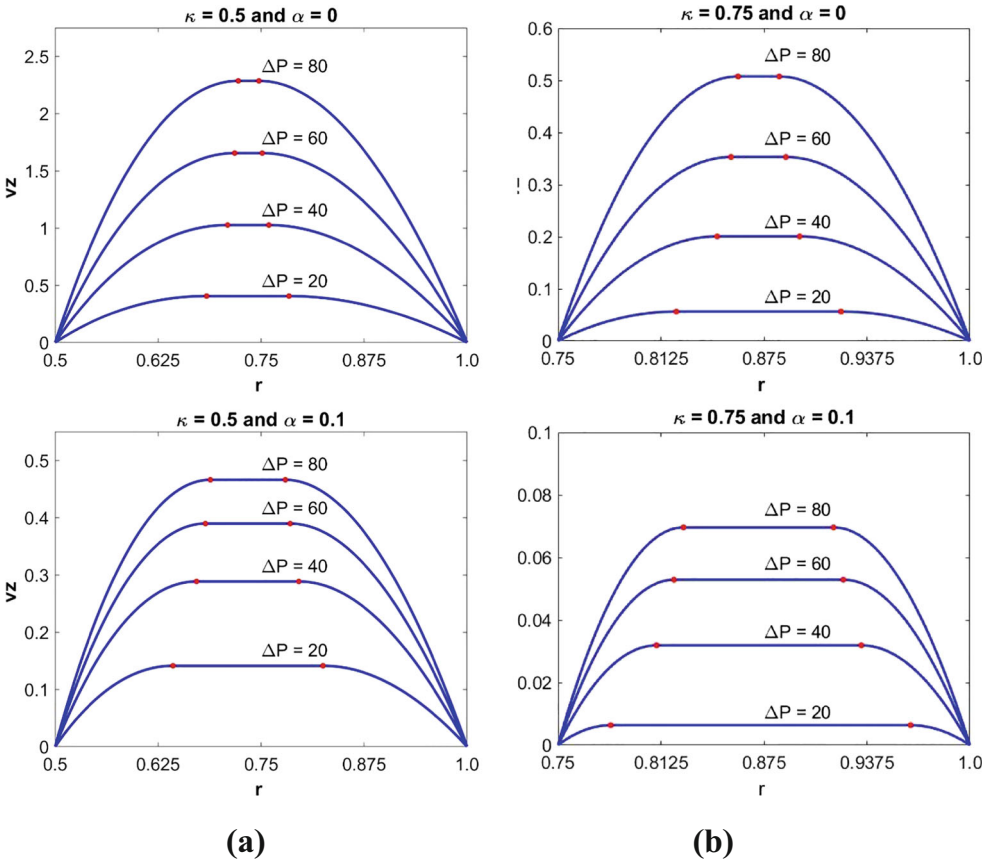

Fig. 7 Velocity distributions (v_z versus the radial distance r) of Bingham plastic flow at different values of the imposed pressure difference for $\varepsilon = 0.01$ and $\alpha = 0$ and 0.1: **a** κ=0.5; **b** κ=0.75. The circles show the positions of the yield points

follows, however, much higher values are employed for α and ε in order to magnify their effects.

As already mentioned and also implied by Eq. (38), when $\alpha > 0$, the pressure is one-dimensional in the unyielded core, varying only with the radial distance z, and two-dimensional in the yielded region. Figure 4 shows the pressure distributions in the unyielded core for $\Delta p = 40$, $\Delta p = 60$ and $\alpha = 0.01$ and 0.1. Interestingly, the pressure distribution in the unyielded core does not depend on the aspect ratio κ of the annulus. As the growth number α increases, the pressure deviates from the linear distribution corresponding to $\alpha = 0$, so that the pressure gradient increases near the inlet plane where the plastic viscosity and the yield stress attain their maximum values and decreases near the exit where both parameters are minimum.

In Fig. 5, the effects of the growth parameter α and the imposed pressure difference Δp on the pressure contours as well as on the radius of the plug for $\varepsilon = 0.01$ and $\kappa = 0.5$ are illustrated. When the aspect ratio ε is low, the pressure in the yielded region remains essentially one dimensional; as a result, the contours are vertical straight lines. The contours are equidistant only when $\alpha = 0$. Otherwise, the distance between the contours increases downstream and this effect is more pronounced as both α and Δp are increased. The two-dimensional character of the flow is exaggerated in Fig. 6 for an annulus with $\kappa = 0.8$ where the rather high value $\varepsilon = 1$ for the aspect ratio has intentionally been chosen. It can be seen that the unyielded region is relatively increased in size as κ decreases or as α increases.

Finally, Fig. 7 shows profiles of v_z versus the radial distance r for $\alpha = 0$ (pressure-independent material parameters) and 0.1 and different values of the imposed pressure difference with $\kappa = 0.5$ and 0.75. As expected, the velocity is reduced as α and κ are increased.

Conclusions

A semi-analytical solution of the fully developed annular flow of an incompressible Bingham plastic, whose rheological parameters vary linearly with pressure, has been derived under the assumption that the growth rates of the yield stress and the plastic viscosity are the same, which is a valid assumption for certain oil drilling fluids. Explicit expressions are provided for the velocity and the pressure distributions in terms of the radii of the unyielded annular core, which are calculated by solving a nonlinear algebraic equation. The pressure difference necessary for initiating the flow increases exponentially with the common dimensionless growth coefficient and decreases with the size of the angular gap. Representative results illustrating the effects of the growth coefficient α and the radii ratio κ on

the pressure distributions and the velocity profiles have been presented and discussed.

Modelling the actual flow of a cutting-laden drilling fluid requires taking into account both temperature and pressure effects as well as the eccentricity of the annulus which can be done only numerically. This is also the case for the isothermal concentric flow when the two growth coefficients are not equal. As already mentioned, in the case of axisymmetric Poiseuille flow, the central unyielded core depends on the relative values of α^* and β^*, i.e., it contracts when $\beta^* < a^*$ and expands when $\beta^* > a^*$. The annular flow, however, is characterized by two yield surfaces; the behavior of which may not be the same depending on the relative values of α^* and β^*. The systematic numerical study of this flow is the focus of our current research efforts.

The solution presented here may be useful in verifying the corresponding codes and providing an upper bound for the frictional losses in an eccentric annulus. It may also be useful in testing numerical simulations of annular Poiseuille flow and lubrication approximation solutions similar to those carried out by Fusi and Farina (2018) and Housiadas et al. (2018) for the flow in a tube of circular cross section.

Acknowledgments Iasonas Ioannou gratefully acknowledges the support of Onassis Foundation.

References

Azar JJ, Roberto Samuel G (2007) Drilling engineering, PennWell Corp

Barus C (1893) Isothermals, isopiestics and isometrics relative to viscosity. Amer J Sci 45:87–96. https://doi.org/10.2475/ajs.s3-45.266.87

Bird RB, Dai GC, Yarusso BJ (1982) The rheology and flow of viscoplastic materials. Rev Chem Eng 1:1–70. https://doi.org/10.1515/revce-1983-0102

Chatzimina M, Xenophontos C, Georgiou G, Argyropaidas I, Mitsoulis E (2007) Cessation of annular Poiseuille flows of Bingham plastics. J Non-Newtonian Fluid Mech 142:135–142. https://doi.org/10.1016/j.jnnfm.2006.07.002

Coussot P (2014) Yield stress fluid flows: a review of experimental data. J Non-Newtonian Fluid Mech 211:31–49. https://doi.org/10.1016/j.jnnfm.2014.05.006

Damianou Y, Georgiou GC (2017) On Poiseuille flows of a Bingham plastic with pressure-dependent rheological parameters. J Non-Newtonian Fluid Mech 250:1–7. https://doi.org/10.1016/j.jnnfm.2017.10.002

Damianou Y, Kaoullas G, Georgiou GC (2016) Cessation of viscoplastic Poiseuille flow in a square duct with wall slip. J Non-Newtonian Fluid Mech 233:13–26. https://doi.org/10.1016/j.jnnfm.2015.11.002

Frigaard I (2019) Simple yield stress fluids. Curr Opin Colloid Interface Sci. https://doi.org/10.1016/j.cocis.2019.03.002

Fusi L, Farina A (2018) Peristaltic axisymmetric flow of a Bingham plastic. Appl Math Comput 320:1–15. https://doi.org/10.1016/j.amc.2017.09.017

Fusi L, Rosso F (2018) Creeping flow of a Herschel-Bulkley fluid with pressure-dependent material moduli. Eur J Appl Math 29(2):352–368. https://doi.org/10.1017/S0956792517000183

Fusi L, Farina A, Rosso F, Roscani S (2015) Pressure-driven lubrication flow of a Bingham fluid in a channel: a novel approach. J Non-Newtonian Fluid Mech 221:66–75. https://doi.org/10.1016/j.jnnfm.2015.04.005

Hermoso J, Martinez-Boza F, Gallegos C (2014) Combined effect of pressure and temperature on the viscous behaviour of all-oil drilling fluids. Oil Gas Sci Technol - Rev IFP Energies Nouvelles 69:1283–1296. https://doi.org/10.2516/ogst/2014003

Housiadas KD, Ioannou I, Georgiou GC (2018) Lubrication solution of the axisymmetric Poiseuille flow of a Bingham fluid with pressure-dependent rheological parameters. J Non-Newtonian Fluid Mech 260:76–86. https://doi.org/10.1016/j.jnnfm.2018.06.003

Huilgol RR, Alexandrou AN, Georgiou GC (2019) Start-up plane Poiseuille flow of a Bingham fluid. J Non-Newtonian Fluid Mech 265:133–139. https://doi.org/10.1016/j.jnnfm.2018.10.009

Ioannou I, Georgiou GC (2018) Axisymmetric Poiseuille flow of a Bingham plastic with rheological parameters varying linearly with pressure. J Non-Newtonian Fluid Mech 259:16–22. https://doi.org/10.1016/j.jnnfm.2018.05.004

Ionescu IR, Mangeney A, Bouchut F, Roche O (2015) Viscoplastic modeling of granular column collapse with pressure-dependent rheology. J Non-Newtonian Fluid Mech 219:1–18. https://doi.org/10.1016/j.jnnfm.2015.02.006

Málek J, Rajagopal KR (2007) Mathematical properties of the solutions to the equations governing the flow of fluids with pressure and shear rate dependent viscosities, in Handbook of mathematical fluid dynamics, Elsevier

Panaseti P, Damianou Y, Georgiou GC, Housiadas KD (2018) Pressure-driven flow of a Herschel-Bulkley fluid with pressure-dependent rheological parameters. Phys Fluids 30:030701. https://doi.org/10.1063/1.5002650

Saramito P, Wachs A (2017) Progress in numerical simulation of yield stress fluid flows. Rheol Acta 56:211–230. https://doi.org/10.1007/s00397-016-0985-9